The impact of size on particle drainage dynamics and antibody response

Simon Zinkhan[1*], Anete Ogrina[2*], Ina Balke[2], Gunta Resevica[2], Andris Zeltins[2], Simone de Brot[3], Cyrill Lipp[1], Xinyue Chang[1], Lisha Zha[4], Monique Vogel[1], Martin F. Bachmann[1,5], Mona O. Mohsen[1,6**]

Affiliations:

[1] Department of BioMedical Research, University of Bern, Bern, Switzerland; Department of Immunology RIA, University Hospital Bern, Bern, Switzerland

[2] Latvian Biomedical Research & Study Centre, Ratsupites iela 1, Riga, LV 1067, Latvia

[3] COMPATH, Institute of Animal Pathology, University of Bern, Bern, Switzerland

[4] International Immunology Center, Anhui Agricultural University, Hefei, Anhui, China.

[5] Jenner Institute, Nuffield Department of Medicine, University of Oxford, UK

[6] Interim Translational Research Institute "iTRI", National Center for Cancer Care & Research Doha, Qatar

[*] Both authors contributed equally to this study

** Correspondence to: Mona O. Mohsen. Email: mona.mohsen@dbmr.unibe.ch

Keywords: virus-like particles, cowpea chlorotic mottle virus, humoral immune response

Abstract

Vaccine-induced immune response can be greatly enhanced by mimicking pathogen properties. The size and the repetitive geometric shape of virus-like particles (VLPs) influence their immunogenicity by facilitating drainage to secondary lymphoid organs and enhancing interaction with and activation of B-cells and other innate humoral immune components. VLPs derived from the plant Bromovirus genus, specifically cowpea chlorotic mottle virus (CCMV), are T=3 icosahedron particles. They can be easily expressed in an *E*. coli host system and package ssRNA during the expression process. Recently, we have engineered CCMV-VLPs by incorporating the universal tetanus toxoid (TT) epitope at the N-terminus. The modified $CCMV_{TT}$-VLPs successfully form icosahedral particles *T=3*, with a diameter of ~30nm analogous to the parental VLPs. Interestingly, incorporating TT epitope at the C-terminus of $CCMV_{TT}$-VLPs results in the formation of Rod-shaped VLPs, ~1µm in length and ~30nm in width. In this study, we have investigated the draining kinetics and immunogenicity of both engineered forms (termed as Round-shaped $CCMV_{TT}$-VLPs and Rod-shaped $CCMV_{TT}$-VLPs) as potential B cell immunogens using different *in vitro* and *in vivo* assays. Our results reveal that Round-shaped $CCMV_{TT}$-VLPs are more efficient in draining to secondary lymphoid organs to charge antigen-presenting cells as well as B-cells. Furthermore, compared to Rod-shaped $CCMV_{TT}$-VLPs, Round-shaped $CCMV_{TT}$-VLPs led to more than 100-fold increased systemic IgG and IgA responses accompanied by prominent formation of splenic germinal centers. Round-shaped $CCMV_{TT}$-VLPs could also polarize the induced immune response towards TH_1. Up to our knowledge, this is the first study investigating and comparing the draining kinetics

44 and immunogenicity of one and the same VLP monomer forming nano-sized icosahedrons or
45 rods in the micrometer size.
46

Introduction

In 1956, Crick and Watson have stated that "it is a striking fact that almost all small viruses are rods or spheres", "These shells are constructed from a large number of identical protein molecules, of small or moderate size, packed together in a regular manner" (1). The main reason for this arrangement is the small genome of viruses, especially RNA viruses. The coat protein (CP) of many viruses is made up of multiple copies arranged in an icosahedron or a helical-shaped geometry (2, 3). The icosahedral structure of viruses is more prevalent than the helical-shaped one.

Virus-like particles (VLPs) have emerged in the last few decades as a premium vaccine platform due to several reasons including: being a safe platform lacking replicating genetic materials, their repetitive surface geometry that serves as a potent pathogen-associated structural pattern (PASP), their ability to package different toll-like receptor ligands (TLRs), the feasibility in coupling different epitopes and most importantly their favorable size ranging between 20-200nm (4). Such size allows VLPs to rapidly and efficiently filter and drain through the conduit system and gain access to lymphoid follicles (4-7). The approved VLP-based vaccines currently on the market mostly exhibit an icosahedral surface geometry based on the quasi-equivalence concept described by Caspar and Klug in 1962 and expressed as *Triangulation (T)* (8, 9). For example, human papilloma viruses (HPVs) are *T=7* of ~60nm in size (10), while hepatitis E virus (HEV) VLPs are *T=1* of ~25nm (11). The different generations of hepatitis B virus (HBV) vaccines show highly organized sub-viral particles (SVPs) of ~20-25nm (12). In contrast, the arrangement of CPs of VLPs in helical or rod-shape geometry is also possible; tobacco-mosaic virus (TMV) is a well characterized representative of this category. Virions of TMV are ~300nm in length and ~18nm in width (13, 14). TMV-VLPs have been investigated as a promising platform in nanotechnology (15) and as a vaccine platform as well (16). Nevertheless, knowledge is scarce regarding TMV-VLPs drainage dynamics. Icosahedral VLPs can be manipulated by inserting few mutations to form rod-shaped VLP. For example, VLPs derived from the bacteriophage Qβ can assemble in a rod-shaped particle following the mutation of five amino acid (a.a.) residues in the FG loop of its CP (17).

It is known that the repetitive surface geometry of icosahedral VLPs enhances optimal induction of B-cell response via cross-linking of B-cell receptors (BCRs) (18, 19). Previously, we have shown that displaying epitopes on icosahedral *T=3* VLPs such as bacteriophage Qβ or plant-derived $CuMV_{TT}$ VLPs result in high specific IgG antibody (Ab) titers as well as neutralizing Abs (20-25). Some studies have revealed that a vaccine based on rod-shaped tobacco-mosaic (TMV)-VLPs could also serve as an effective platform to display different epitopes capable of eliciting an immune response against different pathogens (26, 27).

Cowpea chlorotic mottle virus (CCMV) is a Bromovirus naturally infecting plants and therefore is non-infectious to humans. The infected plants develop yellow spots on their

leaves, hence termed chlorotic (28). The virus is an icosahedron *T=3* of ~28nm in diameter, consisting of 180 sequentially identical CPs. The coat protein can adopt multiple quasi-equivalent forms referred to as the coat subunits A, B and C forming either hexamers (alternating subunits B and C) or pentamers (subunit A). The resulting virus particle consists of 12 pentamers and 20 hexamers (29). Previously, it has been shown that icosahedral CCMV can be converted into rod-shaped particles after a disassembly/reassembly process (30).

In this study, we have demonstrated that CCMV-derived VLPs of different morphology (icosahedral or rod-shaped structure) can be obtained directly from recombinant *E*.coli cells. We specifically manipulated CCMV-VLPs by inserting the universal tetanus toxoid (TT) epitope at the C or N-terminus to form icosahedral VLPs in the nanometer scale or rod-shaped VLPs with sizes in the micron range. Such intervention allowed us to study the impact of size on particles in terms of drainage dynamic and magnitude of induced immune response using VLPs based on essentially the same VLP-monomer. Our results demonstrate for the first time that VLPs in the nm size range are vastly more immunogenic than micron-sized particles.

Materials and methods:

Round-shaped and Rod-shaped $CCMV_{TT}$-VLPs cloning, expression and production

Cloning of CCMV-CP with induced tetanus toxoid epitope for expression: A cloned copy of the CCMV coat protein gene (wt *CP)* was obtained from Dr. Alain Tissot (Zürich) and used in PCR mutagenesis for insertion of the coding sequence of tetanus toxoid epitope (TT830 – 843; QYIKANSFIGITE) in 5'- and 3'- terminal ends of the CP gene. To replace the original amino acids at the N-terminus of CCMV CP with the TT epitope sequence, the pET42-CCMVwt plasmid was used as a template for PCR amplification and mutagenesis. *NdeI* site at the 5'end of the CCMVwt gene was used for cloning corresponding PCR products. To introduce the tetanus toxoid epitope coding sequence into the CCMV-wt gene, two step PCR mutagenesis was necessary. For the first step amplification the following primers were used for N terminal PCR: CC_N83_d24F (5'ATACATATGGGCCAGTATATTAAGGCCAACTCCAAATTTATCGGGATTACCGA 3') and CC_N83R (5' AGTTAACTTCCCTGTACCGACTGTTTCGGTAATCCCGATAAATTTGGAGTTG 3').

For the second round the PCR products from the first round were diluted 1:50 and re-amplified with primers CC_N83_d24F and CC_AgeR (5' ACTTCGATACGCTGTAACCGGTCCA 3').

For C terminal insertion of TT epitope the following primers were used: CC_C83F (5' TGACGACTCTTTCACTCCGGTCTATGGCCAGTATATTAAGGCCAACTCC 3') and CC_C83R (5' TTACTCGAGAAGCTTATTACTCGGTAATCCCGATAAATTTGGAGTTG 3'). Second round of the PCR was performed as describe above using primers CC_C83R (5'

TTACTCGAGAAGCTTATTACTCGGTAATCCCGATAAATTTGGAGTTG 3') and CC_SacIIF (5' CCCTTGAACAACTCGCCGCGGA 3').

The corresponding PCR fragments were analysed in 0.8% agarose gel and then purified using the *GeneJet Gel Extraction* kit (Thermo Fischer Scientific, Waltham, Massachusetts). Then the 5' terminal end PCR product and plasmid pET42-CCMVwt were digested with enzymes *NdeI* and *BshTI* (Thermo Fischer Scientific, Waltham, Massachusetts) and ligated, resulting in plasmid pET42-CCMV-Ntt830. The 3'terminal end PCR product and plasmid pET42-CCMVt were digested with enzymes *Cfr42I* and *XhoI* (Thermo Fischer Scientific, Waltham, Massachusetts) and ligated, resulting in plasmid pET42-CCMV-Ctt830.

E.coli XL1-Blue cells were used as a host for cloning and plasmid amplification. To avoid PCR errors several CP gene-containing pET42 plasmid clones were sequenced using the BigDye cycle sequencing kit and an ABI Prism 3100 Genetic analyzer (Applied Biosystems, Carlsbad, USA). After sequencing, the plasmid clones without sequence errors were chosen for further experiments.

Cloning of CCMV-SS-CP with induced tetanus toxoid epitope for expression: To obtain "salt-stable" CCMV VLPs, the replacement of lysine against arginine in position 42 (K42R) was necessary. For CCMVwt-SS the following primers were used: CCP_salt_AgeI_R (5' TGTAACCGGTCCATGCTTTAATAGCGCGGCCTT 3') and CCM_NdeF (5' ATACATATGTCTACAGTCGGTACAGGG 3'). For CCMV-Ntt830-SS the following primers were used: CC_N83_d24F and CC_salt_AgeI_R. The corresponding PCR products were cloned into the pTZ57R/T vector (Thermo Fischer Scientific, Waltham, Massachusetts). *E. coli* XL1-Blue cells were used as a host for cloning and plasmid amplification. To avoid RT-PCR errors, several CP gene-containing pTZ57 plasmid clones were sequenced using the BigDye cycle sequencing kit and an ABI Prism 3100 Genetic analyser (Applied Biosystems, Foster City, California). After sequencing, corresponding DNA fragments without sequence errors were subcloned into the *NdeI/AgeI* sites of pET42-CCMVwt and pET42-CCMV-Ntt830 expression vectors, resulting in the expression plasmids pET42-CCMV-SS and pET42-CCMV-Ntt830-SS. For C terminal tetanus toxoid CCMV-SS construct the corresponding *NdeI/BsrGI*-fragment from pET42-CCMV-SS was subcloned into pET-CCMV-Ctt830, generating the expression vector pET42-CCMV-Ctt830-SS.

Expression and purification of CCMV-SS VLPs: To obtain all salt stable CCMV CP VLPs, each construct was transformed and expressed in *E. coli* C2566 cells (New England Biolabs, Ipswich, USA). After selection of clones with the highest expression levels of the target protein, *E. coli* cultures were grown in 2xTY medium containing kanamycin (25 mg/l) on a rotary shaker (200 rev/min; Infors, Bottmingen, Switzerland) at 30°C to an OD600 of 0.8–1.0. Then, expression was induced with 0.2 mM Isopropyl-β-D-thiogalactopyranoside (IPTG), and the medium was supplemented with 5 mM $MgCl_2$ and 2 mM $CaCl_2$. Incubation was

continued on the rotary shaker at 20°C for 18 h. The resulting biomass was collected by low-speed centrifugation and was frozen at -70°C. After thawing on ice, the cells were suspended in buffer containing 15 mM sodium phosphate pH 7.5 supplemented with 150 mM NaCl (buffer A) with additional 0.5 mM urea, 1 mM PMSF, 5 mM mercapto-ethanol, and were disrupted by ultrasonic treatment. Insoluble proteins and cell debris were removed by centrifugation (13,000 rpm, 30 min at 5°C). All steps involved in the expression of VLP were monitored by SDS-PAGE using 12.5% gels.

CCMV-SS and CCMV-Ctt830-SS VLPs were separated from cellular proteins by ultracentrifugation (SW28 rotor, Beckman, Palo Alto, USA; at 25,000 rpm, 6 h, 5°C) in a sucrose gradient (20–60% sucrose in buffer A, without mercapto-ethanol and urea, supplemented with 0.5% Triton X-100). The content of gradient tubes was divided into six fractions, starting at the bottom of the gradient, and the fractions were analysed by SDS-PAGE. Fractions containing CCMV-SS CP proteins were combined and dialyzed against 100 volumes of buffer A to remove the sucrose. If necessary, samples were concentrated using an Amicon Ultra-15 centrifugal device (Millipore, Cork, Ireland).

However, soluble proteins of CCMV-Ntt830-SS were precipitated using a mixture of PEG 8,000 (8%) and NaCl (0.15 M), collected by centrifugation and dissolved in buffer A. PEG/NaCl precipitation was repeated for CCMV-Ntt830-SS. After solubilisation or dialysis (in case of CCMV-SS), all CCMV CP preparations were purified two times using an ultracentrifuge and 30% sucrose cushion – first with additional 0.5% Triton X-100 and the second time without Triton X-100 (4 h, 50 000 rmp, 4°C; Type 70Ti rotor, Beckman) and the pellet was then dissolved in buffer A. If necessary, samples were concentrated using an Amicon Ultra-15 centrifugal device (Millipore, Cork, Ireland). To obtain pure preparations of CCMV-CPs for subsequent electron microscopy (EM) analysis, stability and immunological studies, the sucrose gradient, dialysis, and concentration steps were repeated.

All steps involved in the expression and purification of VLP were monitored by SDS-PAGE (using 12.5% gels). The concentration of purified CCMV–CPs were estimated using the QuBit fluorometer in accordance with manufacturer's recommendations (Invitrogen, Carlsbad, California). Concentrated VLP solutions were stored at +4°C.

Electron microscopy

Purified Round-shaped or Rod-shaped $CCMV_{TT}$-VLPs proteins (1 mg/ml) were adsorbed on carbon formvar-coated copper grids and were negatively stained with 0.5% uranyl acetate aqueous solution. The grids were examined using a JEM-1230 electron microscope (JEOL, Tokyo, Japan) at an accelerating voltage of 100 kV.

Mass Spectrometry

Wild type $CCMV_{TT}$-VLPs, Round or Rod-shaped $CCMV_{TT}$-VLPs (1 mg/ml in buffer A) were diluted with a 2,5-Dihydroxyacetophenone (2,5-DHAPI) matrix solution and were spotted onto

an MTP AnchorChip 400/384TF. Matrix assisted laser desorption/ionization (MALDI)-TOF MS analysis was carried out on an Autoflex MS (Bruker Scientific, Billerica, Massachusetts). The protein molecular mass (MM) calibration standard II (22.3–66.5 kDa; Bruker, Billerica, Massachusetts) was used for mass determination.

SDS-Page and gel electrophoresis

SDS-Page: 6µg of Round or Rod-shaped $CCMV_{TT}$-VLPs were mixed with 2x mercaptoethanol and heated at 95°C for 3 minutes and then loaded into Any kD Mini-PROTEAN TGX precast protein gels (BIO-RAD). Gel was run for 35min at 180V. As reference Page Ruler™ Prestained Protein Ladder was used (Thermo Fisher Scientific, Waltham, Massachusetts). Gel electrophoresis: 10µg of Round- or Rod-shaped $CCMV_{TT}$-VLPs were loaded on a 1% agarose gel. Nucleic acids were visualized using Cybr Safe DNA Gel Stain (Life Technologies, Carlsbad, California). 5µl Quick-Load Purple 1 kb DNA ladder (New England Biolabs, Ipswich, Massachusetts) was used as reference. Gel was run for 30min at 100V.

Mice

Wild type C57BL/6 mice were purchased from Harlan. All *in vivo* experiments were performed using 8-12 weeks old female mice. All animal procedures were conducted in accordance with the Swiss Animal Act (455.109.1 – September 2008, 5th).

Vaccination regimen

Wild type C57BL/6 mice (8-12 weeks, Harlan) were vaccinated subcutaneously (SC) with 15µg Round or Rod-shaped $CCMV_{TT}$-VLPs in 100µl PBS on day 0. Mice were boosted with a identical dose on day 14. Serum samples were collected on days 0, 7, 14, 21, 28 and 35.

The enzyme-linked immunosorbent assay (ELISA)

For determination of total IgG antibody titers against Round and Rod-shaped $CCMV_{TT}$-VLPs in sera of immunized mice, ELISA plates (Nunc Immuno MaxiSorp, Rochester, NY) were coated over night with Round or Rod-shaped $CCMV_{TT}$-VLPs, respectively. Plates were washed with PBS-0.01%Tween and blocked using 100µl PBS-Casein 0.15% for 2h. Sera from immunized mice were diluted 1/20 initially and a 1/3 dilution chain was performed. Plates were incubated for 1h at 37°C. After washing with PBS-0.01%Tween, goat anti-mouse IgG conjugated to Horseradish Peroxidase (HRP) (Jackson ImmunoResearch, West Grove, Pennsylvania) was added 1/1000 and incubated for 1h at 37°C. Plates were developed and OD 450 reading was performed.

IgG subclasses were measured from day 21 sera using the same ELISA protocol with the following secondary Abs: goat anti-mouse IgG1-HRP (BD Biosciences, San Jose, California), goat anti-mouse IgG2b-HRP (1:1000) (Thermo Fischer Scientific, Waltham, Massachusetts), goat anti-mouse IgG2c-HRP (Southern Biotech, Birmingham, Alabama) 1:4000, rat anti-mouse IgG3-biotin (Becton, Dickinson, Franklin Lakes, New Jersey) 1:2000 followed by streptavidin-HRP (Dako, Glostrup, Denmark) 1:1000 incubated at 37°C for 1h.

IgA was measured using day 35 sera (immunization at day 0, boost at day 14). IgG was depleted using Dynabeads™ Protein G (Thermo Fischer Scientific, Waltham, Massachusetts). Serum was diluted 1/20 (total volume of 75µl) in PBS-Casein 0.15%. 25µl beads were used per sample. Manufacturer's protocol was followed until step 3. of "Bind Antibody". Supernatant was added to ELISA plates and a 1/3 serial dilution was performed. For IgA detection, goat anti mouse IgA conjugated to HRP was used (ThermoFisher Scientific, Waltham, Massachusetts) 1/4000.

For OD50 calculations, if a sample did not reach the threshold a value of 1 was appointed.

Measuring IFN- γ in mouse serum

Wild type C57BL/6 mice (8-12 weeks, Harlan) were vaccinated with 15µg Round or Rod-shaped $CCMV_{TT}$-VLPs on day 0 and boosted on day 14. Serum from vaccinated mice was collected for measuring IFN- γ. ELISA MAX™ Deluxe Set Mouse IFN-γ (Biolegend, San Diego, California) was performed according to manufacturer's instructions. Serum was used undiluted and concentration was interpolated to a standard curve of the sets standard sample.

Trafficking of Round and Rod-shaped $CCMV_{TT}$-VLPs to draining lymph nodes

Round or Rod-shaped $CCMV_{TT}$-VLPs were labelled with AF488 as per manufacturer's instructions (Thermo Fischer Scientific, Waltham, Massachusetts) and stored at -20°C. Wild type C57BL/6 mice (8-12 weeks, Harlan) were injected with 10µg of the VLPs in the footpad under isoflurane anesthesia. Popliteal LNs were collected 3h and 24h following footpad injection. Lymph nodes were treated with collagenase D (Roche, Basel, Switzerland) and DNase I (Boehringer, Ingelheim am Rheih, Germany) in DMEM medium containing 5% FBS and 1% Strep/Penicillin for 30 min at 37°C. Lymph nodes were smashed using 70µm cell strainers, RBC were lysed with ACK buffer. Cells were stained with Fc blocker and then with anti-CD11b, CD11c, CD45R/220, CD8 and F4/80 (all from Biolegend, San Diego, California).

Immunofluorescence

Round or Rod-shaped $CCMV_{TT}$-VLPs were labelled with AF488 as per manufacturer's instructions (Thermo Fischer Scientific, Waltham, Massachusetts) and stored at -20°C. Wild type C57BL/6 mice (8-12 weeks, Harlan) were injected with 10µg of the VLPs in the footpad under isoflurane anesthesia. Popliteal LNs were collected 3h and 24h following footpad injection and embedded in Tissue-Tek optimum cutting temperature compound (Sakura) without prior fixation. Cryostat sections (7µm in thickness) on Superforst/Plus glass slides (Thermo Fischer Scientific, Waltham, Massachusetts) were air-dried overnight and then fixed for 10 min in ice-cold 100% acetone (PanReac). After rehydration (5 min in 1x PBS), sections were blocked with 1% (w/v) BSA (Sigma Aldrich, St. Louis, Missouri) and 1% (v/v) normal mouse serum. Immunofluorescence labeling was done with Abs diluted in PBS containing 0.1% (w/v) BSA and 1% (v/v) normal mouse serum. Sections were washed 3 times for 5 min in 1x PBS after every labeling step. LN staining: macrophages were detected using a primary

antibody against CD11b (1/1000, rat anti mouse CD11b conjugated with PE; BD Biosciences, San Jose, California), B-cell follicles were identified using rat anti mouse B220 Alexa F647 (1/1000; BD Biosciences, San Jose, California). Images were acquired on an Axioplan microscope using an AxioCam MRn (Zeiss).

Histology of lymph node

Round or Rod-shaped $CCMV_{TT}$-VLPs were labelled with AF488 as per manufacturer's instructions (Thermo Fischer Scientific, Waltham, Massachusetts) and stored at -20. Wild type C57BL/6 mice (8-12 weeks, Harlan) were injected with 10µg of the VLPs in the footpad under isoflurane anesthesia. Popliteal LNs were collected 3h and 24h following footpad injection and fixed with 4% paraformaldehyde solution (Sigma Aldrich, St. Louis, Missouri). Of each group, two to four murine popliteal LNs were histologically examined by a board-certified veterinary pathologist (SdB). Of each LN, a full cross section, stained with Hematoxylin and Eosin (HE), was assessed for any histopathological changes.

Statistical analysis

Data were analyzed and presented as mean ± SEM using GraphPad PRISM 8. Comparison between the groups was performed using Student's *t*-test. *P*-values $^{****}P < 0.0001$; $^{***}P < 0.001$; $^{**}P < 0.01$; $^{*}P < 0.05$.

Results:

Directional insertion of tetanus toxoid (TT) epitope in the N or C-terminal results in Round or Rod-shaped $CCMV_{TT}$-VLPs

In a first step, we engineered CCMV-VLPs derived from a non-human pathogenic plant virus by incorporating a powerful T-cell stimulatory epitope derived from tetanus toxoid (TT) (Tetanus toxin 830-843) at the N or C-terminus of CCMV-VLPs. The TT epitope was genetically fused to the capsid protein (CP) of CCMV-VLPs as has been previously described for our newly developed platform derived from cucumber-mosaic virus-like particles ($CuMV_{TT}$-VLPs) (31). The introduced TT epitope is considered a universal epitope in humans as it is recognized by essentially all individuals. Since all individuals have been immunized against TT, memory Th cells may be able to help B cells to generate protective IgG even under more challenging conditions such as aged populations (31). CCMV-VLPs with insertion of TT epitope at the N-terminus retain their self-assembly as an icosahedron similar to the native virus. In contrast, insertion of TT epitope at the C-terminal end led to formation of Rod-shaped particles. Both Round and Rod-shaped CCMV-VLPs forms carry a lysine to arginine mutation at residue 42 (32). This mutation renders the VLPs less sensitive to pH and salt concentration, which is an advantage in *in vivo* environments (A. Zeltins, manuscript in preparation). Therefore, the engineered VLPs in this study are salt-stable (SS). The shape and integrity of the cloned VLPs were confirmed via electron microscopy which shows a size of ~30nm in

diameter for CCMV-Ntt-SS (Fig. 1a). The size of the $CCMV_{TT}$-Ctt-SS greatly varies in length but can reach up to more than 1µm, with a width of about 30nm. Figure 1b shows a magnified image of $CCMV_{TT}$-Ctt-SS VLPs for easy comparison of their width with the icosahedral $CCMV_{TT}$-Ntt-SS VLPs in figure 1a. To reach a rather homogenous population, we performed sucrose gradient separation to focus on the long rods (Fig. 1c). For simplification we refer to the two forms of engineered $CCMV_{TT}$ in this paper as Round-shaped $CCMV_{TT}$-VLPs (CCMV-Ntt-SS) and Rod-shaped $CCMV_{TT}$-VLPs (CCMV-Ctt-SS).

To further characterize the two forms of $CCMV_{TT}$, we performed mass spectrometry (MS). MS data revealed a molecular weight for the CP monomers of Round- and Rod-shaped $CCMV_{TT}$-VLPs of roughly 21.8 and 21.9kDa, respectively (Fig. 1d). The original CCMV-SS (salt-stable CCMV without TT insertion) is formed by CPs of roughly 20.2kDa. Considering the weight of the TT 830-843 epitope of 1.611kDa the obtained data are consistent. Reducing SDS-page experiments confirmed these findings and showed bands for Round- and Rod-shaped $CCMV_{TT}$-VLPs of equal height at the appropriate position (Fig. 1e).

Both engineered $CCMV_{TT}$-VLPs were produced in an *E*. coli system. The VLPs packaged ssRNA derived from *E*. coli spontaneously, which serves as a potent TLR7/8 ligand. The concentration of RNA in both Round- and Rod-shaped $CCMV_{TT}$-VLPs was similar when measured at 260nm. The RNA content of the Round-shaped $CCMV_{TT}$-VLPs could also be visualized by agarose gel electrophoresis, however this was less efficient for the Rod-shaped $CCMV_{TT}$-VLPs because most of the RNA staying in the slot based on the Rod-shaped $CCMV_{TT}$-VLPs being unable to move through the gel (Fig. 1f).

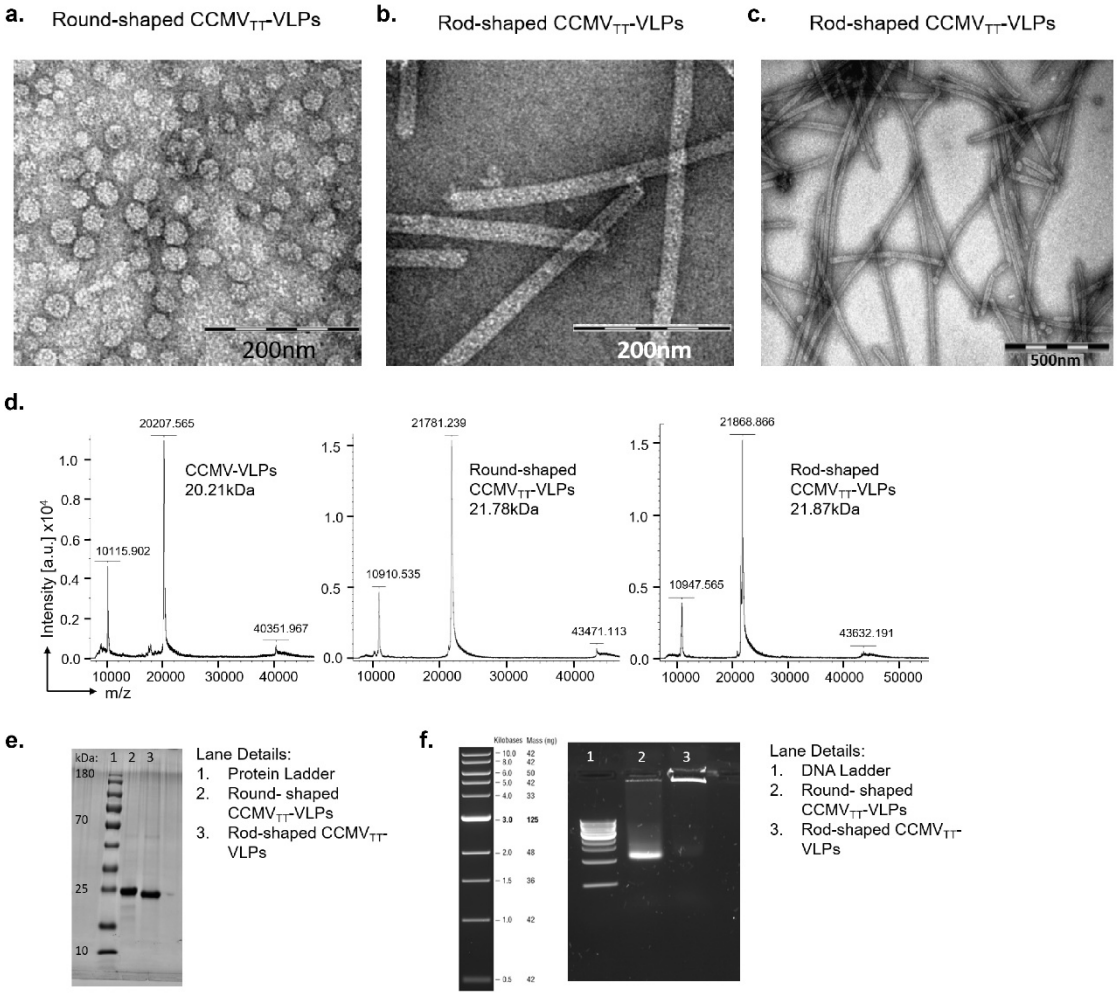

Figure 1: Directional insertion of tetanus toxoid (TT) epitope in the N or C-terminal results in Round or Rod-shaped CCMV$_{TT}$-VLPs. a, EM of Round-shaped and ***b./c.*** Rod-shaped CCMV$_{TT}$-VLPs, adsorbed on carbon grids and negatively stained with uranyl acetate solution, scale bars 200nm (Round) and 200nm/500nm (Rod). Round-shaped CCMV$_{TT}$-VLPs are ~30nm in diameter, Rod-shaped CCMV$_{TT}$-VLPs are ~1µm in length and ~30nm in width. ***d***, Mass spectrometry data, from left to right: wild type CCMV$_{TT}$-VLPs, Round-shaped CCMV$_{TT}$-VLPs and Rod-shaped CCMV$_{TT}$-VLPs. ***e***, Reducing SDS-Page stained with Coomassie-blue stain, lane 1: protein marker, lane 2: Round-shaped CCMV$_{TT}$, lane 3: Rod-shaped CCMV$_{TT}$. ***f***, Agarose gel stained with SYBR safe, lane 1: DNA ladder, lane 2: Round-shaped CCMV$_{TT}$, lane 3: Rod-shaped CCMV$_{TT}$.

Round-shaped CCMV$_{TT}$-VLPs exhibit faster and more efficient draining kinetics than Rod-shaped CCMV$_{TT}$-VLPs in vivo

To test the role of size and shape in lymphatic trafficking of the engineered VLPs, we assessed and visualized the accumulation of the AF488 labelled Round or Rod-shaped CCMV$_{TT}$-VLPs in murine popliteal lymph nodes (LNs) 3h and 24h after injection in the

footpads. Flow cytometry data confirms that Round-shaped $CCMV_{TT}$-VLPs were more efficient in reaching the popliteal LNs than the Rod-shaped ones. Such finding is not surprising as the round VLPs have a size of ~30nm in diameter allowing them to drain freely through the 200nm pores of the lymphatic vessels. Nevertheless, the Rod-shaped $CCMV_{TT}$-VLPs were also capable of draining through the lymphatic vessels within 3 hours, despite their micro-size, this may be due to the fact that the width of the rods is ~30nm, similar to the diameter of the round-shaped $CCMV_{TT}$-VLPs.

Next, we studied which type of APCs are involved in interacting with the Round and Rod-shaped $CCMV_{TT}$-VLPs. Lymph node conventional dendritic cells (cDCs); $CD8^+CD11c^+$ (Fig. 2a), $CD8^-CD11c^+$ (Fig. 2b), macrophages $CD11b^+F4/80^+$ (Fig. 2c), different myeloid cells populations $CD45^+CD11b^+$ (Fig. 2d and h), neutrophils $CD45^+$ $Ly6G^+$ (Fig. 2e) and B cells $CD45R/B220^+$ (Fig. 2f and i) were more efficient in taking up Round-shaped than Rod-shaped $CCMV_{TT}$-VLPs 3h after injection. No significant difference in the uptake between Round and Rod-shaped $CCMV_{TT}$-VLPs has been seen at 24h except for B cells and the macrophage population characterized by $CD11b^+F4/80^+$ (Fig. 2c). Interestingly, uptake by those macrophages was more prominent for Rod-shaped than Round-shaped $CCMV_{TT}$-VLPs 24h post injection. This might result from delayed drainage of Rod-shaped $CCMV_{TT}$-VLPs. B cells characterized by $CD45R/B220^+$ showed a very high frequency in taking up Round-shaped $CCMV_{TT}$-VLPs in the popliteal LNs 3h and 24h after injection in the mouse footpad. B cells taking up $CCMV_{TT}$-VLPs also showed expression of MHC-II (Fig. 2f and g). We next followed the arrival of the labelled $CCMV_{TT}$-VLPs to the draining LNs by fluorescence microscopy of cryosections obtained from excised popliteal LNS at 3h and 24h post injection in the mouse footpad. The sections were co-stained with macrophage and B-cell markers, $CD11b^+$ and $CD45^+/B220^+$, respectively. The results demonstrate that AF488 Round-shaped $CCMV_{TT}$-VLPs accumulated in large numbers in the subcapsular sinus area (SCS), the cortex and the medullary sinus (MS) of the popliteal LNs 3h post injection (Fig. 2j). Macrophages characterized with $CD11b^+$ were prominent 3h post injection with Round-shaped $CCMV_{TT}$-VLPs at the SCS and MS. Rod-shaped $CCMV_{TT}$-VLPs were less visible 3h at the popliteal LN post injection in the footpad and their presence was confined to the SCS with scarce VLPs in the cortex. 24h post injection, Round-shaped $CCMV_{TT}$-VLPs were found deeper in the popliteal LN. Whereas, this observation was less obvious for the Rod-shaped $CCMV_{TT}$-VLPs. B-cells were detectable 3h and 24h post injection of the VLPs in the mouse footpads. As the accumulation of Round-shaped $CCMV_{TT}$-VLPs was prominent 3h post injection in the footpad, the B-cell signal was less noticeable. 24h later the accumulation of B-cells was more pronounced at the SCS and the cortical area of the LN upon injection of Round-shaped $CCMV_{TT}$-VLPs than after injection with Rod-shaped $CCMV_{TT}$-VLPs.

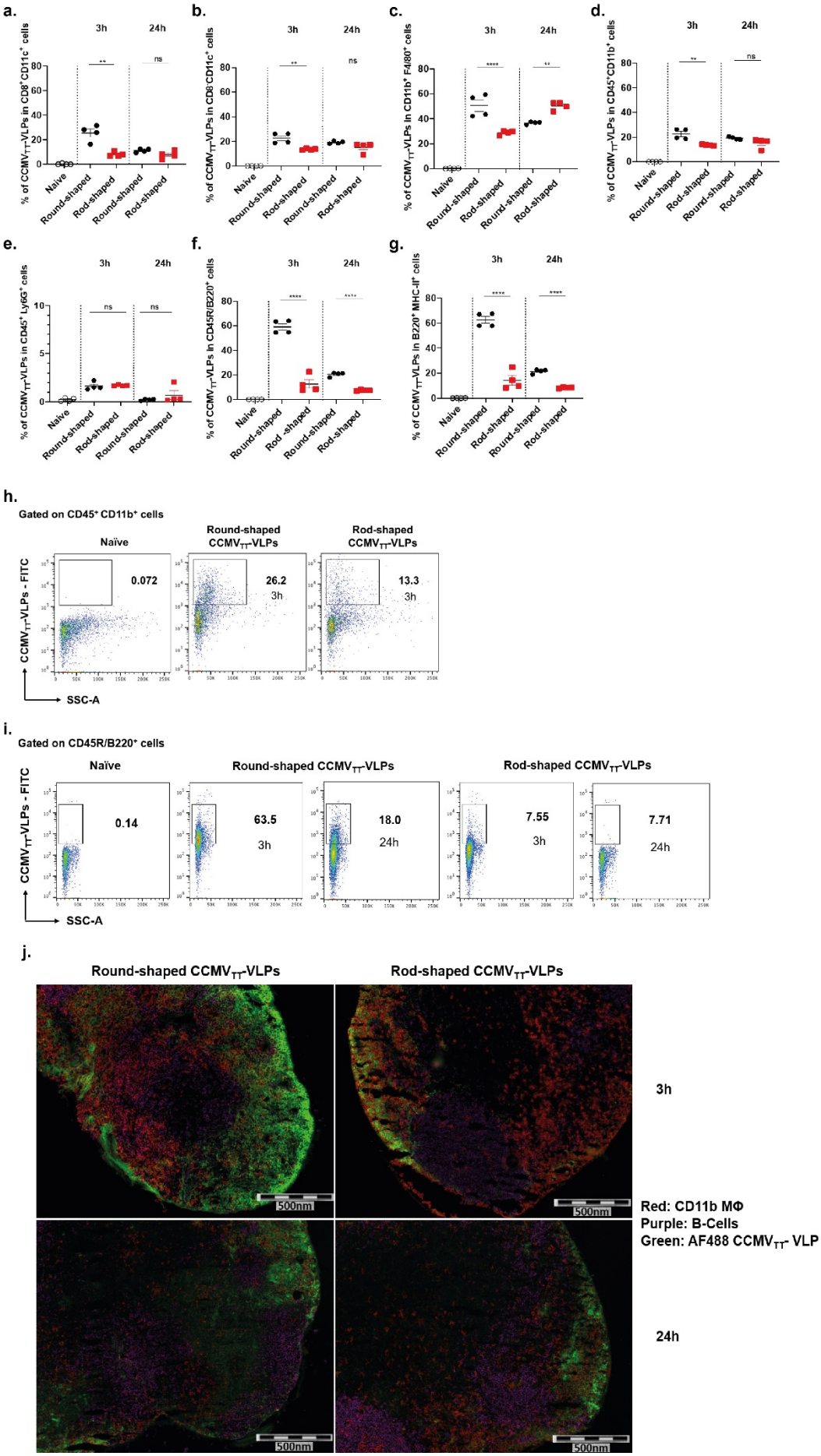

Figure 2*: *Round-shaped CCMV$_{TT}$-VLPs exhibit faster and more efficient draining kinetics than Rod-shaped CCMV$_{TT}$-VLPs in vivo. Percentage of different cell populations positive for AF488 labeled Round and Rod-shaped CCMV$_{TT}$-VLPs in murine popliteal LNs 3h and 24h post injection in footpad: ***a***, CD8$^+$CD11c$^+$ cells; ***b***, CD8$^-$CD11c$^+$ cells; ***c***, CD11b$^+$F4/80$^+$ cells; ***d***, CD45$^+$CD11b$^+$ cells. ***e***, CD45$^+$Ly6G$^+$ cells; ***f***, CD45R/B220$^+$ cells and ***g***, CD45R/B220$^+$ MHC$^+$ cells. ***h***, Representative FACS plots showing the percentage of CCMV$_{TT}$-VLPs labelled with AF488 in CD45$^+$CD11b$^+$ cells in popliteal LNs 3h post injection in mouse footpad. ***i***, Representative FACS plot showing the percentage of CCMV$_{TT}$-VLPs labelled with AF488 in CD45R/B220$^+$ cells in popliteal LNs 3h and 24h post injection in mouse footpad. Naïve LNs were used as a negative control. ***j***, Immunofluorescence of popliteal LNs 3h and 24h post vaccination with Round or Rod-shaped CCMV$_{TT}$-VLPs labeled with AF488, cyrosections were treated with Abs detecting CD11b$^+$ cells (red colour) and CD45/B220$^+$ cells (purple colour). Mean ± SEM, 4 mice per group, one representative of 2 similar experiments is shown.

Round-shaped CCMV$_{TT}$-VLPs are more potent in inducing IgG antibodies than Rod-shaped CCMV$_{TT}$-VLPs

In a next step, we have assessed the humoral immune response induced by both engineered Round and Rod-shaped CCMV$_{TT}$-VLPs. It is important to keep in mind that it is usually difficult to compare different sized particles for their immunogenicity as for spheres, the surface is proportional to radius $(r)^2$, while the weight will be proportional to $(r)^3$. Hence the weight of the injected particles grows much more rapidly than the surface, rendering a comparison difficult. In contrast, for rods, both the surface and weight are proportional to the length of the rod, rendering this comparison more appropriate.

Hence, C57BL/6 mice were vaccinated subcutaneously (SC) with 15µg of Round or Rod-shaped CCMV$_{TT}$-VLPs on day 0 and boosted once on day 14 as illustrated in Figure 3a. Serum was collected on day 0 before vaccination and subsequently on day 7, 14, 21, 28 and 35. Total specific IgG response against Round or Rod-shaped CCMV$_{TT}$-VLPs was assessed by ELISA. As shown in Fig. 3b and c, the Round-shaped CCMV$_{TT}$-VLPs were very potent at inducing specific IgG response 7 days following the administration of the first dose. This response was enhanced dramatically on days 14, 21, 28 and 35. On the contrary, vaccination with Rod-shaped CCMV$_{TT}$-VLPs was low after the first dose and has been increasing significantly only following boost on day 14.

Even though subunits of both VLPs were almost identical, in order to test the cross-reactivity of both Round and Rod-shaped CCMV$_{TT}$-VLPs, we have tested the collected sera in ELISA coated with the opposite VLP shape. Specifically, sera from mice vaccinated with Round-shaped CCMV$_{TT}$-VLPs were tested against ELISA coated with Rod-shaped CCMV$_{TT}$-VLPs and vice versa. Our results showed that sera from mice vaccinated with Round-shaped CCMV$_{TT}$-VLPs are capable of recognizing the Rod-shaped CCMV$_{TT}$-VLPs after a single dose on day 7. The response was enhanced on day 14, 21, 28 and 35. However, sera from mice

vaccinated with Rod-shaped CCMV$_{TT}$-VLPs could only significantly recognize the Round-shaped CCMV$_{TT}$-VLPs after boosting (Fig. 3d and e). In a next step, we have produced Rod-shaped CCMV$_{TT}$-VLPs exhibiting variation in lengths that includes smaller fragmented pieces of less than ~1µm in length (By ways of using polyethylene glycol precipitation instead of sucrose gradient centrifugation for purification, as described for Round-shaped CCMV$_{TT}$-VLPs

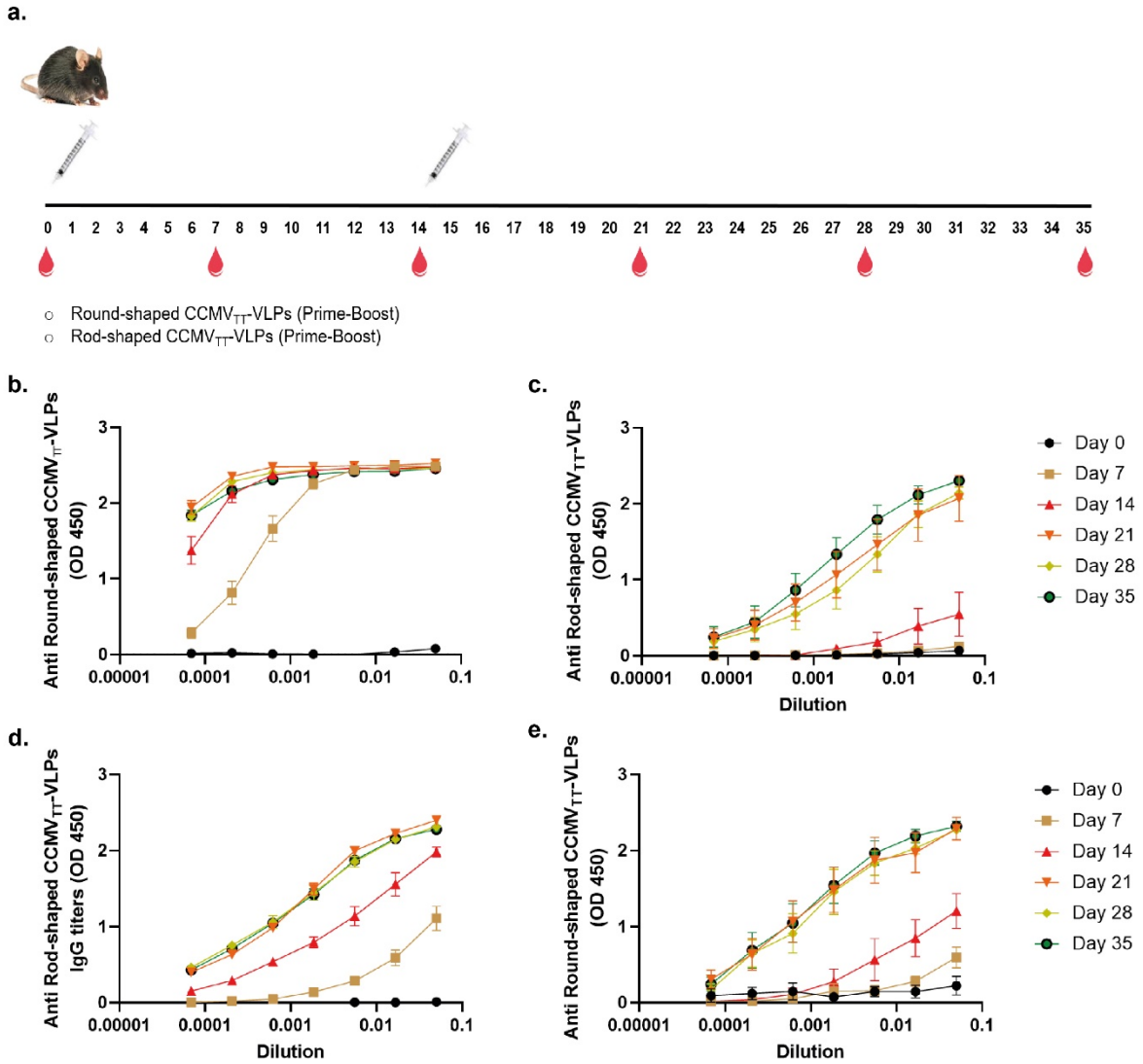

Figure 3: Round-shaped CCMV$_{TT}$-VLPs are more potent in inducing IgG antibodies than Rod-shaped CCMV$_{TT}$-VLPs. a, Vaccination regimen and bleeding time-points. ***b***, Sera from Round-shaped CCMV$_{TT}$-VLP vaccinated mice, ELISA plates coated with Round-shaped CCMV$_{TT}$-VLPs. ***c***, Sera from Rod-shaped CCMV$_{TT}$-VLP vaccinated mice, ELISA plates coated with Rod-shaped CCMV$_{TT}$-VLPs. ***d***, Sera from Round-shaped CCMV$_{TT}$-VLP vaccinated mice, ELISA plates coated with Rod-shaped CCMV$_{TT}$-VLPs. ***e***, Sera from Rod-shaped CCMV$_{TT}$-VLP vaccinated mice, ELISA plates coated with Round-shaped CCMV$_{TT}$-VLPs. Mean ± SEM, 6 mice per group, one representative of 2 similar experiments is shown.

in material & methods; Supplementary Fig. 1). Specific anti-IgG response against the Rod-shaped CCMV$_{TT}$-VLPs was enhanced substantially, indicating that indeed the rod-length limited the size of the immune response (Supplementary Fig. 2). In all other experiments presented in this paper the more homogeneous long Rod-shaped CCMV$_{TT}$-VLPs were used.

Rod-shaped CCMV$_{TT}$-VLPs fail to induce isotype switching in comparison to the Round-shaped CCMV$_{TT}$-VLPs

The C57BL/6 murine IgG family consists of four major subclasses IgG1, IgG2b, IgG2c and IgG3. Each unique subclass is implicated in distinct effector functions during humoral immune responses. VLPs and other nanoparticles induce a humoral response dominated by IgG1 in the absence of packaged RNA or DNA in mice (26, 33, 34). Isotype switching to the protective IgG2 subtype is strictly TLR dependent. Thus, VLPs packaged with prokaryotic ssRNA during *E*. coli production induce a humoral immune response dominated with IgG2 subclasses (35, 36). Based on these grounds, we were interested in characterizing the different IgG subclasses in mice sera vaccinated with Round vs Rod-shaped CCMV$_{TT}$-VLPs. As explained earlier the engineered Round and Rod-shaped CCMV$_{TT}$-VLPs package the same quantity of ssRNA. Therefore, TLR7/8 ligand effect can be eliminated as a confounding variable and the difference in the induced IgG subclasses can be correlated to the size of the VLPs. Our analysis revealed that Round-shaped CCMV$_{TT}$-VLPs significantly enhanced all IgG subclasses compared to the Rod-shaped ones. The difference, however, was most striking for TLR7/8 related subclasses IgG2b/c and IgG3 (Fig.4a). By performing OD50 analysis we compared the titers (given as reciprocal dilution values) in both groups as depicted in Figure 4b. Titers are significantly higher (p. <0.0001 for IgG1, IgG2b and IgG2c) (p. <0.05 for IgG3) post immunization with Round-shaped CCMV$_{TT}$-VLPs. The ratio between TH_1 and TH_2 associated IgG subclasses was calculated next and it became evident that TH_1 contribution is more pronounced with Round-shaped CCMV$_{TT}$-VLPs (Fig. 4c).

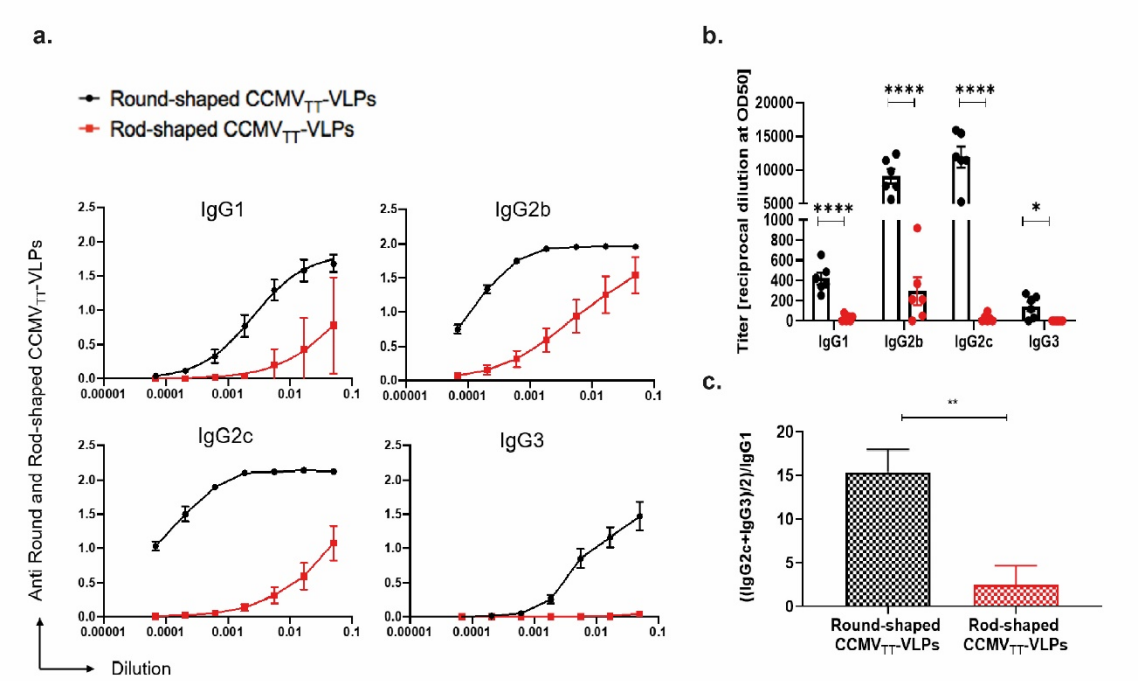

Figure 4: Rod-shaped CCMV$_{TT}$-VLPs fail to induce isotype switching in comparison to the Round-shaped CCMV$_{TT}$-VLPs. ***a***, Anti-Round and Rod-shaped CCMV$_{TT}$-VLP specific IgG1, IgG2b, IgG2c and IgG3 titers measured in day 21 mice sera using OD450nm. ELISA plates were coated with Round-shaped CCMV$_{TT}$-VLPs for detecting IgG subclasses in mice vaccinated with Round-shaped CCMV$_{TT}$-VLPs. ELISA plates were coated with Rod-shaped CCMV$_{TT}$-VLPs for detecting IgG subclasses in mice vaccinated with Rod-shaped CCMV$_{TT}$-VLPs. ***b***, Anti-Round and Rod-shaped CCMV$_{TT}$-VLP specific IgG1, IgG2b, IgG2c and IgG3 titers measured in day 21 mice sera using OD50 calculation of data depicted in a. ***c***, TH_1/TH_2 ratio in Round and Rod-shaped CCMV$_{TT}$-VLP immunized mice depicted as ((IgG2c+IgG3)/2)/IgG1 of OD50 values shown in b. Mean ± SEM, 6 mice per group, one representative of 2 similar experiments is shown.

Systemic IgA response depends on size of VLPs

Previous studies have shown that SC injection of VLPs packaging RNA leads to a strong IgA response despite the fact that IgA antibodies are TH-cell independent (35). Besides, our previous findings revealed that systemic IgA response is heavily dependent on TLR7/8 in B-cells (37). The role of the size of VLPs packaging similar contents of RNA has not been investigated before, therefore we carried out an experiment to investigate this matter. Our findings indicate that Round-shaped CCMV$_{TT}$-VLPs could induce significantly higher (*p*. <0.0001) isotype switching to IgA when compared to the Rod-shaped ones (Fig. 5a and b). To rule out the role of TH-cells, we have also measured IFN-γ in the serum of vaccinated mice on day 14, the results showed no significant difference (*p*. 0.8211) between both groups (Fig. 5c).

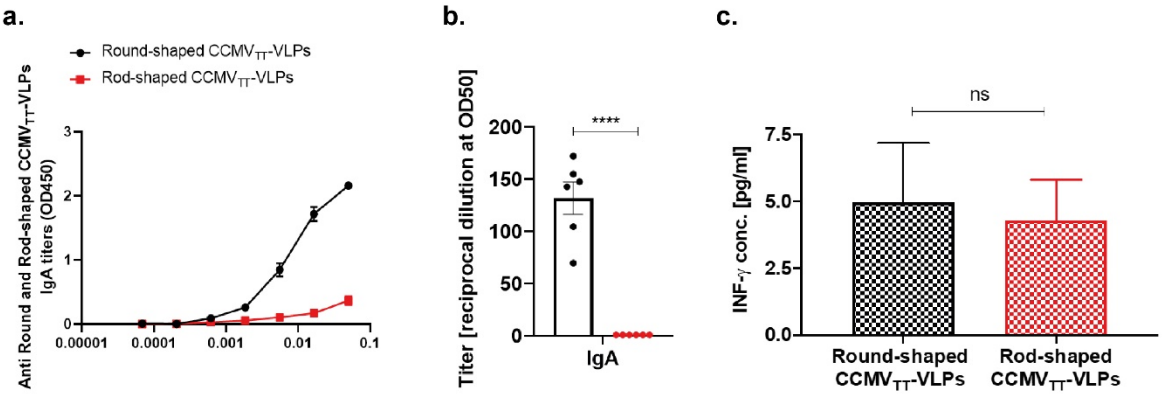

Figure 5. Systemic IgA response depends on size of VLPs. a, Anti-Round and Rod-shaped CCMV$_{TT}$-VLP specific IgA titers measured in day 21 serum from mice vaccinated with Round and Rod-shaped CCMV$_{TT}$-VLPs using OD450nm. ***b***, Anti-Round and Rod-shaped CCMV$_{TT}$-VLP specific IgA titers measured using OD50 calculation of data depicted in a. ***c***, Concentration of IFN-γ measured in day 14 serum from mice vaccinated with Round and Rod-shaped CCMV$_{TT}$-VLPs. Mean ± SEM, 6 mice per group, one representative of 2 similar experiments is shown.

Germinal center formation is prominent following a single dose of Round-shaped CCMV$_{TT}$-VLPs

Antigen reservoir persisting on follicular dendritic cells (fDCs) is essential for germinal centers (GC) to keep B-cells stimulated and to generate a strong and long-lived antibody response. We therefore studied the formation of GCs in the spleens of mice vaccinated with Round and Rod-shaped CCMV$_{TT}$-VLPs 12 days following a single SC dose of the engineered VLPs. Results showed that the formation of GCs in mice vaccinated with Round- shaped CCMV$_{TT}$-VLPs was significantly higher than in Rod-shaped CCMV$_{TT}$-VLP vaccinated mice when measuring the total number of GCs (*p*. 0.0042) or the number of GCs/mm^2 (*p*. 0.0033) (Fig. 6a and b). Histological examination of Hematoxylin and Eosin (HE) stained splenic tissue indicated the presence of multiple GCs within the lymphoid follicles upon vaccination with Round-shaped CCMV$_{TT}$-VLPs. On the other hand, mice vaccinated with Rod-shaped CCMV$_{TT}$-VLPs revealed only rare GC formation. Spleens from naïve C57BL/6 mice were used as a control (Fig. 6c and d). The examined spleens in mice vaccinated with Round or Rod-shaped CCMV$_{TT}$-VLPs were free of any relevant degenerative or necrotic histopathological changes.

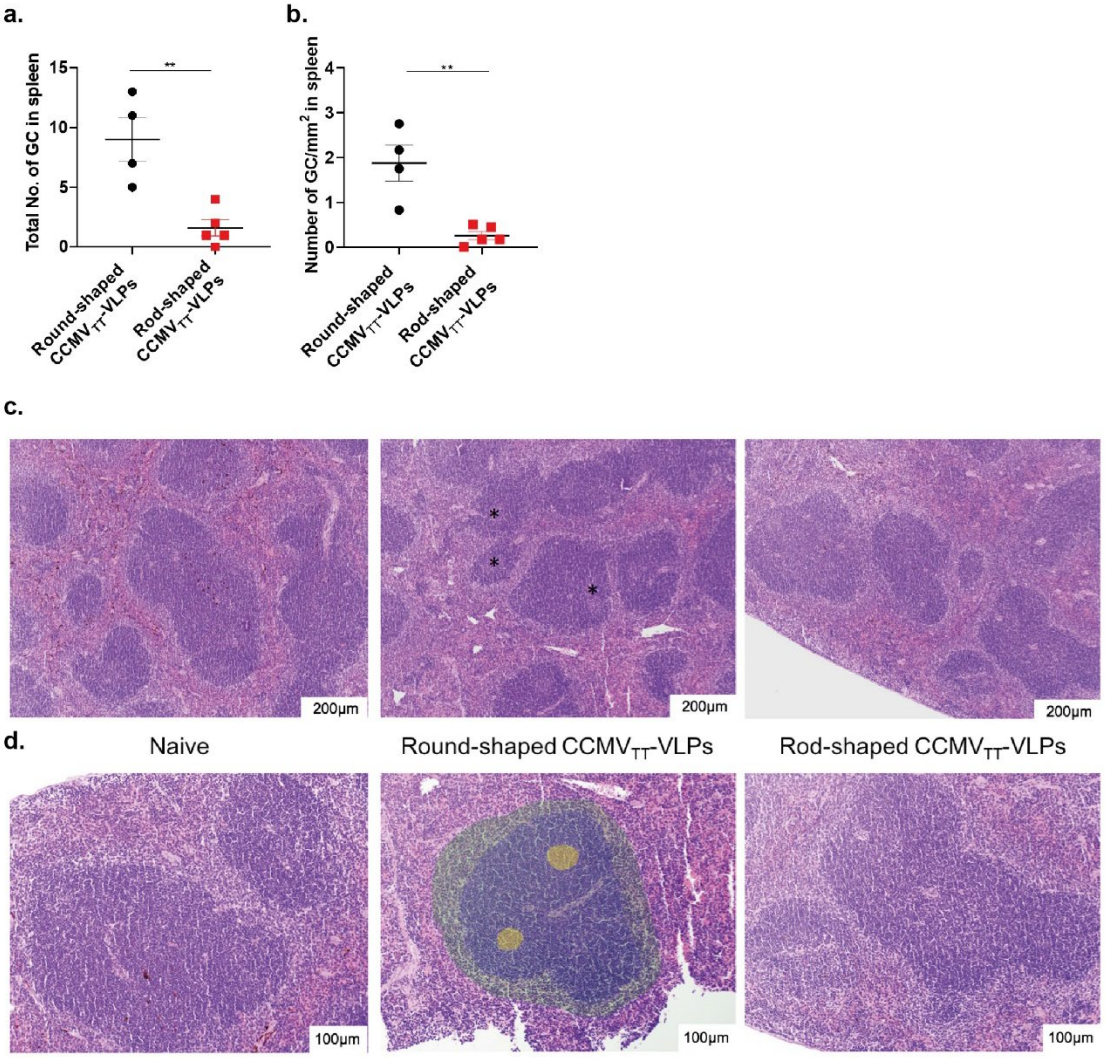

Figure 6: Germinal center formation is prominent following a single dose of Round-shaped CCMV$_{TT}$-VLPs. ***a***, Total number of germinal centers (GCs) in the examined splenic tissue fragments of mice vaccinated with a single dose of 15µg of Round or Rod-shaped CCMV$_{TT}$-VLPs. ***b***, Number of GCs/mm^2 in spleen of mice vaccinated with a single dose of 15µg of Round-shaped CCMV$_{TT}$-VLPs. ***c***, Histology of HE stained murine spleens, 10x objective. From the left: naïve spleen, lymph follicles lack evident GC formation; spleen of mice vaccinated with Round-shaped CCMV$_{TT}$-VLPs, lymph follicle present multifocal GC formation (*); last spleen of mice vaccinated with Rod-shaped CCMV$_{TT}$-VLPs, lymph follicle lack visible GCs. ***d***, Higher magnification of c., 20x objective. From the left: naïve spleen, lymph follicles present with densely arranged lymphocytes without evident GC formation; spleen of mice vaccinated with Round-shaped CCMV$_{TT}$-VLPs, GCs (*) are visible within the lymph follicles, GCs and surrounding follicular and perifollicular zones are highlighted with colours (GCs (yellow), mantle zone (blue) and marginal zone (green)); last spleen of mice vaccinated with Rod-shaped CCMV$_{TT}$-VLPs, lymph follicles present with densely arranged lymphocytes without evident GC formation. Mean ± SEM, 2 splenic tissue fragments were analyzed from naïve group, 4 from Round-shaped CCMV$_{TT}$-VLPs group and 5 from Rod-shaped CCMV$_{TT}$-VLPs group.

Round and Rod-shaped CCMV$_{TT}$-VLPs enhance neutrophil infiltration in lymph node sinuses without causing any degenerative or vascular changes.

To study the histopathological effect of Round and Rod-shaped CCMV$_{TT}$-VLPs on LNs, we have performed histology of HE stained popliteal LNs collected 3h and 24h following footpad injections. The main histopathological change of the examined LNs was restricted to a mild to moderate increase of neutrophils within the sinuses, which was present in both groups and absent or neglectable in control tissue (Table 1 and Fig. 7a-c). This neutrophil infiltrate was more evident 3h than 24h after injection. No convincing histological difference was observed between the two groups vaccinated with Round or Rod-shaped CCMV$_{TT}$-VLPs. Evidence of tissue damage, i.e. degeneration or necrosis, was not observed. The observed results were consistent with the previous flow cytometry data in Figure 2e which did not show any statistical difference in the percentage of AF488-labelled VLPs taken up by neutrophils characterized by CD11b^{+}Ly6G^{+} 3h or 24h post injection in the footpad.

Table 1. Summary of the relevant histopathological changes in the examined popliteal LNs, indicated per treatment group.

Group	**Time**	**Neutrophil infiltrate**		
		Absent or neglectable	**Mild**	**Moderate**
Naive	-	1/1 (100%)	0/1	0/1
Naive	-	1/1 (100%)	0/1	0/1
Round-shaped CCMV$_{TT}$-VLPs	3h	0/3	0/3	3/3 (100%)
Rod-shaped CCMV$_{TT}$-VLPs	3h	0/2	0/2	2/2 (100%)
Round-shaped CCMV$_{TT}$-VLPs	24h	0/4	2/4 (50%)	2/4 (50%)
Rod-shaped CCMV$_{TT}$-VLPs	24h	0/4	2/4 (50%)	2/4 (50%)

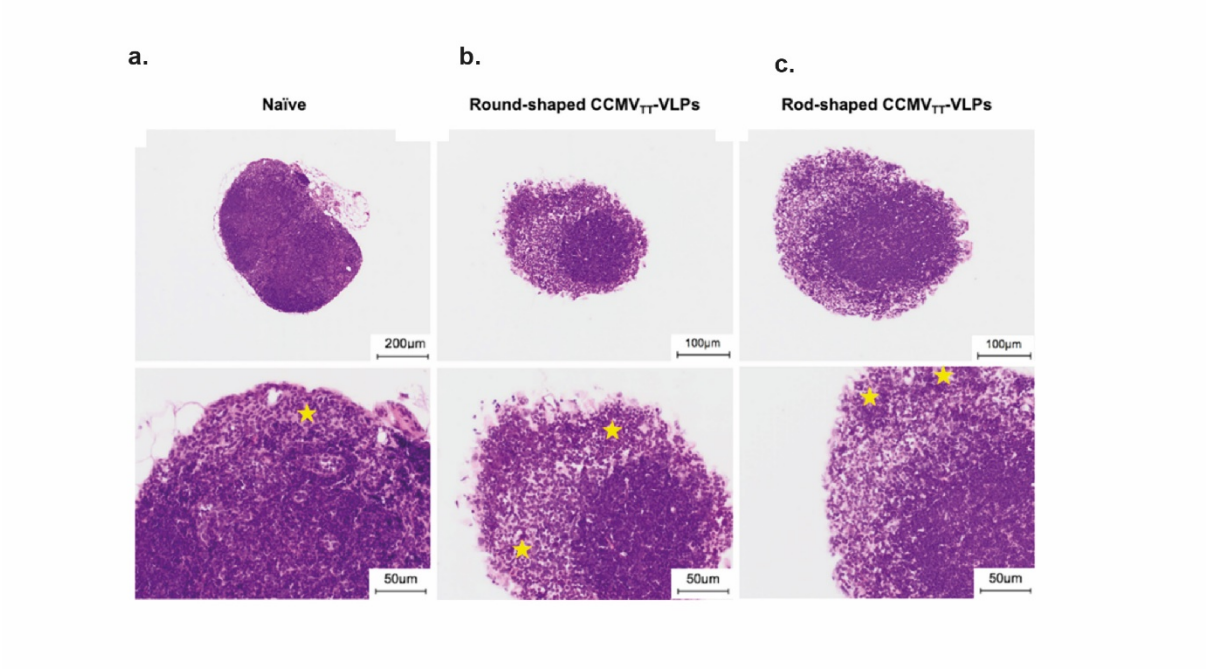

Figure 7. Round and Rod-shaped CCMV$_{TT}$-VLPs enhance neutrophil infiltration in lymph node sinuses without causing any degenerative or vascular changes. a, Top: Naïve popliteal LN 10x objective, HE stain, Bottom: Closer view of Naïve popliteal LN. Within the sinuses (*), granulocytes are rare. 40x objective, HE stain. ***b***, Top: Popliteal LN, 3h after footpad injection with Round-shaped CCMV$_{TT}$-VLPs. 20x objective, HE stain, Bottom: Closer view of popliteal LN, 3h after footpad injection with Round-shaped CCMV$_{TT}$-VLPs. Moderate predominantly neutrophil infiltration in the subcapsular sinus (*). 40x objective, HE stain. ***c***, Top: Popliteal LN, 3h after footpad injection with Rod-shaped CCMV$_{TT}$-VLPs, 20x objective, HE stain. Bottom: Closer view of popliteal LN, 3h after footpad injection with Rod-shaped CCMV$_{TT}$-VLPs. Moderate predominantly neutrophil infiltration in the subcapsular sinus (*). 40x objective, HE stain.

Discussion

In the current study we have engineered VLPs with nearly identical primary sequence but fundamentally different structural properties; one forming round icosahedrons with a diameter of around 30nm while the other formed rods of about ~1µm. To this end, we inserted a universal tetanus toxoid (TT) epitope at the N or C-terminus of cowpea chlorotic mottle virus (CCMV)-VLPs. The insertion of TT epitope at the N-terminus did not interfere with the original parental structure and resulted in icosahedral particles T=3; named in this study as Round-shaped CCMV$_{TT}$-VLPs. However, inserting TT epitope at the C-terminus of CCMV$_{TT}$-VLPs caused the formation of Rod-shaped CCMV$_{TT}$-VLPs of ~1µm in length and ~30nm in width. As both engineered VLPs were expressed in *E*. coli, they packaged a similar quantity of ssRNA serving as TLR7/8 agonists recognized by PRRs for effective stimulation of the innate immune system. This allowed us to study the impact of size on drainage dynamics and the magnitude of the induced immune responses with one and the same VLP monomer while

567 excluding the effect of TLR7/8 ligands. As mentioned above, both the surface and mass of
568 rods are proportional to the diameter and length, allowing to vary the surface exposed to B
569 cells with a proportional change in mass.
570 B-cell activation by antigens is a critical step for effective initiation of the adaptive
571 immune response (38). Particulate antigens like VLPs can be passively or actively transported
572 to the lymphoid organs following injection. The passive transportation is based on their ability
573 to drain freely through the lymphatic vessels since they have an ideal size of ~30-50nm. Our
574 previous studies have proven that icosahedral VLPs such as bacteriophage Qβ-VLPs and
575 VLPs derived from cucumber-mosaic virus (CuMV-VLPs) can freely reach the draining LN in
576 less than a minute, both having a size of ~30nm (6, 7, 39). By contrast, particulate antigens
577 larger than 500nm cannot efficiently enter the lymphatic capillaries (40, 41). Instead, they need
578 to be actively transported via specialized cells (42). To visualize the trafficking kinetics of the
579 engineered Round and Rod-shaped $CCMV_{TT}$-VLPs (~30nm and ~1µm) respectively, they
580 were labelled with AF488 and injected in mouse footpads. Flow cytometric analysis and
581 cryosections of the popliteal LNs 3h and 24h post injection were performed. The results
582 demonstrate more efficient drainage of the Round-shaped $CCMV_{TT}$-VLPs via the lymphatic
583 vessels, which have pores of ~200nm, 3h following injection in the footpad in comparison with
584 the Rod-shaped ones. Nevertheless, Rod-shaped $CCMV_{TT}$-VLPs have also been detected in
585 the draining popliteal LN 3h post injection in the mouse footpad. This observation may be
586 explained by 2 scenarios: 1) Rod-shaped $CCMV_{TT}$-VLPs exhibit a width of ~30nm which may
587 allow them to drain into the lymphatic capillaries despite their length. Indeed, if spheres of
588 >500nm size are used for injection, these spheres required 24 hours to arrive in LNs and fully
589 depend on cellular transport (43) and 2) our FACS analysis data indicates that neutrophils
590 characterized by $CD11b^+$ $Ly6G^+$ can also actively transport both engineered VLPs in a similar
591 manner.
592 Different subsets of APCs participated in uptake Round or Rod-shaped $CCMV_{TT}$-VLPs upon
593 injection in mouse footpads. Both lymphoid-resident DCs, $CD8^+CD11c^+$ and $CD8^-CD11c^+$,
594 were more efficient at transporting Round-shaped $CCMV_{TT}$-VLPs. Generally, $CD8^+$ DCs are
595 more potent in cross-presenting VLP-derived antigens (44). The subcapsular sinus
596 macrophages are considered the frontline cells to capture pathogens in the draining LN and
597 retain them from entering the LN parenchyma. Afterwards they relay the antigen to B-cells for
598 efficient priming and induction of humoral immune responses (45). Yolanda, et al. proposed a
599 model for particulate-antigen acquisition by B-cells. The model suggests that particulate
600 antigens firstly accumulate in the macrophage-niche area in the SCS of the draining LN
601 followed by a still unknown filtration process of the antigens to the follicle. Next, non-antigen
602 specific B-cells carry particulate antigens from the SCS to be deposited on FDCs (39). Our

603 fluorescent microscopy cryosections could demonstrate such findings as Round-shaped
604 $CCMV_{TT}$-VLPs were more efficient in draining to the popliteal LNs 3h post injection in the
605 mouse footpad where macrophages could also be abundantly observed. 24h later the Round-
606 shaped $CCMV_{TT}$-VLPs could be detected deeper in the LN. The binding of the Round-shaped
607 $CCMV_{TT}$-VLPs by B-cells was significantly higher (*p*. <0.0001) when compared to the Rod-
608 shaped $CCMV_{TT}$-VLPs, both at 3h and 24h post injection in the footpad as shown using FACS
609 analysis. This is consistent with our previous observation that Round-shaped VLPs bind to B
610 cells in a complement and CD21-dependent manner (46).
611 The repetitive surface geometry of VLPs enhance their cross-linking to B-cells and
612 ability to activate complement (38). T=3 VLPs are capable of cross-linking 180 BCRs resulting
613 in a strong humoral immune response. T=3 VLPs may be favorable over T=1 as the later can
614 cross-link ~60 BCRs which is at the threshold for an optimal immune response (47). However,
615 data are scarce in regard to rod-shaped VLPs and their ability to activate B cells. In this study,
616 we show that a single priming injection of Round-shaped $CCMV_{TT}$-VLPs was efficient at
617 inducing a high specific Ab titer which was further enhanced upon boosting on day 14. On the
618 contrary, the Rod-shaped $CCMV_{TT}$-VLPs could only induce a specific Ab response following
619 boosting on day 14 which remained much reduced compared to the Round-shaped VLP
620 induced response. These results were confirmed by the significantly increased formation of
621 total no. of GCs (*p*. 0.0042) as well as no. of GCs/mm^2 (*p*. 0.0033) in spleens 12 days following
622 vaccination with Round-shaped $CCMV_{TT}$-VLPs.
623 When testing the vaccinated mice sera against the opposite engineered VLPs, Round-
624 shaped $CCMV_{TT}$-VLPs were also more efficient in recognizing the Rod-shaped ones even
625 after a single dose. These data indicate that icosahedral VLPs are capable of inducing specific
626 Ab directed against other forms of the same VLPs in an efficient manner and that 30nm sized
627 round VLPs are far superior over 1µm sized rods.
628 To achieve successful IgG class-switching and memory formation in B cells, co-
629 delivery of innate immune stimuli is crucial (18). It has been shown that class-switching to
630 IgG2a/c and IgG2b is dependent on simultaneous engagement of BCR and TLR9 after
631 immunization with particulate antigens (48, 49). Furthermore, TLR7 engagement with different
632 RNA types influenced the outcome of the humoral immune response to VLP immunization.
633 Bacterial RNA pointed the immune response toward IgG2 production, whereas eukaryotic
634 RNA induced responses favored high IgG1 titers (50). IgG1 is associated with TH_2 responses,
635 whereas IgG2a/c and IgG3 is associated with TH_1 responses even though TLR-signaling in B
636 cells is key for IgG subclass induction. The obtained data reveal that Round-shaped $CCMV_{TT}$-
637 VLPs were more efficient than the rod-shaped at inducing class-switching. Furthermore, the
638 ratio between TH_1 and TH_2 associated IgG subclasses was more significant (*p*. 0.0045) when

vaccinating with Round-shaped $CCMV_{TT}$-VLPs, indicating that rod-shaped VLPs are less effective at driving TLR7-signaling.

Similar to IgG2a responses, VLPs packaged with RNA lead to a strong systemic IgA response. We have shown previously that IgA response is TH cell independent (35) and requires TLR7/8 or 9 to induce a systemic response (37). Here, we show that the systemic IgA response measured on day 21 using a SC prime-boost regimen was much higher in mice vaccinated with Round-shaped $CCMV_{TT}$-VLPs than in mice vaccinated with Rod-shaped $CCMV_{TT}$-VLPs (*p*. <0.0001). Hence, these results also support that TLR7-signaling in B cells is inferior if rods are used for immunization.

The histologic analysis of LNs after immunization with either Round or Rod-shaped $CCMV_{TT}$-VLPs showed an increased number of predominantly neutrophils which were interpreted to correspond to draining leukocytes through the sinuses. The term 'infiltrate' is preferred over the term 'inflammation' (i.e. lymphadenitis) due to the lack of degenerative or vascular changes in the examined LNs (51, 52). Neutrophil infiltrate was more evident in the tissues sampled 3h than in those sampled 24h post injection, in agreement with the known rapid recruitment of these cells to sites of infection or tissue injury and the short half-lives of neutrophils (53). Increased numbers of neutrophils were absent or neglectable in the examined control LN tissue, which makes a background lesion unlikely. No evident histological difference was observed between the LNs corresponding to the two groups of Round or Rod-shaped $CCMV_{TT}$-VLPs, indicating that both types of VLPs effectively recruit neutrophils.

Taken together, our data demonstrate that antigen size is a key determinant of immunogenicity and that icosahedral antigens of ~30nm in diameter are far more immunogenic than essentially the same viral capsid protein assembled into µm sized rods. Trafficking from injection site to LNs as well as trafficking within LNs and direct interaction with B cells explain the difference.

Acknowledgment:

This work was supported by Qatar National Research Fund (PDRA grant PDRA4-0118-18002), the Swiss National Science Foundation (SNF 310030_185114 and SNF 310030_179165) and by Latvian Science Council (Grant No. lzp-2019/1-0131).

Declaration of interests:

The authors declare no competing interests

References

1. Crick FH, Watson JD. Structure of small viruses. Nature. 1956;177(4506):473-5.
2. Caspar DL. Movement and self-control in protein assemblies. Quasi-equivalence revisited. Biophys J. 1980;32(1):103-38.
3. Louten J. Essential Human Virology2017. 344 p.

4. Gomes AC, Mohsen M, Bachmann MF. Harnessing Nanoparticles for Immunomodulation and Vaccines. Vaccines (Basel). 2017;5(1).
5. Gretz JE, Norbury CC, Anderson AO, Proudfoot AE, Shaw S. Lymph-borne chemokines and other low molecular weight molecules reach high endothelial venules via specialized conduits while a functional barrier limits access to the lymphocyte microenvironments in lymph node cortex. J Exp Med. 2000;192(10):1425-40.
6. Mohsen MO, Gomes AC, Cabral-Miranda G, Krueger CC, Leoratti FM, Stein JV, et al. Delivering adjuvants and antigens in separate nanoparticles eliminates the need of physical linkage for effective vaccination. J Control Release. 2017;251:92-100.
7. Mohsen MO, Heath MD, Cabral-Miranda G, Lipp C, Zeltins A, Sande M, et al. Correction to: Vaccination with nanoparticles combined with micro-adjuvants protects against cancer. J Immunother Cancer. 2019;7(1):137.
8. Caspar DL, Klug A. Physical principles in the construction of regular viruses. Cold Spring Harb Symp Quant Biol. 1962;27:1-24.
9. Mohsen MO, Augusto G, Bachmann MF. The 3Ds in virus-like particle based-vaccines: "Design, Delivery and Dynamics". Immunol Rev. 2020.
10. Wang JW, Roden RB. Virus-like particles for the prevention of human papillomavirus-associated malignancies. Expert Rev Vaccines. 2013;12(2):129-41.
11. Guu TS, Liu Z, Ye Q, Mata DA, Li K, Yin C, et al. Structure of the hepatitis E virus-like particle suggests mechanisms for virus assembly and receptor binding. Proc Natl Acad Sci U S A. 2009;106(31):12992-7.
12. Ho JK, Jeevan-Raj B, Netter HJ. Hepatitis B Virus (HBV) Subviral Particles as Protective Vaccines and Vaccine Platforms. Viruses. 2020;12(2).
13. Chapman ML, L. Advances in Protein Chemistry2003. 1-253 p.
14. Ge P, Zhou ZH. Hydrogen-bonding networks and RNA bases revealed by cryo electron microscopy suggest a triggering mechanism for calcium switches. Proceedings of the National Academy of Sciences. 2011;108(23):9637.
15. Zhang Y, Dong YX, Zhou JH, Li X, Wang F. Application of Plant Viruses as a Biotemplate for Nanomaterial Fabrication. Molecules. 2018;23(9).
16. Balke I, Zeltins A. Recent Advances in the Use of Plant Virus-Like Particles as Vaccines. Viruses-Basel. 2020;12(3).
17. Cielens I, Ose V, Petrovskis I, Strelnikova A, Renhofa R, Kozlovska T, et al. Mutilation of RNA phage Qbeta virus-like particles: from icosahedrons to rods. FEBS Lett. 2000;482(3):261-4.
18. Jennings GT, Bachmann MF. The coming of age of virus-like particle vaccines in: Biological Chemistry Volume 389 Issue 5 (2008). Biological Chemistry, Volume 389: Issue 52008.
19. Jennings GT, Bachmann MF. Immunodrugs: Therapeutic VLP-Based Vaccines for Chronic Diseases. Annual Review of Pharmacology and Toxicology: Annual Reviews; 2009. p. 303-26.
20. Cabral-Miranda G, Lim SM, Mohsen MO, Pobelov IV, Roesti ES, Heath MD, et al. Zika Virus-Derived E-DIII Protein Displayed on Immunologically Optimized VLPs Induces Neutralizing Antibodies without Causing Enhancement of Dengue Virus Infection. Vaccines (Basel). 2019;7(3).
21. Olomski F, Fettelschoss V, Jonsdottir S, Birkmann K, Thoms F, Marti E, et al. Interleukin 31 in insect bite hypersensitivity-Alleviating clinical symptoms by active vaccination against itch. Allergy. 2020;75(4):862-71.
22. Fettelschoss-Gabriel A, Fettelschoss V, Olomski F, Birkmann K, Thoms F, Buhler M, et al. Active vaccination against interleukin-5 as long-term treatment for insect-bite hypersensitivity in horses. Allergy. 2019;74(3):572-82.

726 23. Thoms F, Jennings GT, Maudrich M, Vogel M, Haas S, Zeltins A, et al.
727 Immunization of cats to induce neutralizing antibodies against Fel d 1, the major feline
728 allergen in human subjects. J Allergy Clin Immunol. 2019;144(1):193-203.
729 24. Storni F, Zeltins A, Balke I, Heath MD, Kramer MF, Skinner MA, et al. Vaccine
730 against peanut allergy based on engineered virus-like particles displaying single major peanut
731 allergens. J Allergy Clin Immunol. 2020;145(4):1240-53.e3.
732 25. Cabral-Miranda G, M Salman A, O Mohsen M, L Storni F, S Roesti E, A Skinner M,
733 et al. DOPS Adjuvant Confers Enhanced Protection against Malaria for VLP-TRAP Based
734 Vaccines. Diseases (Basel, Switzerland). 2018;6(4):107.
735 26. Pogue GP, Lindbo JA, Garger SJ, Fitzmaurice WP. Making an ally from an enemy:
736 plant virology and the new agriculture. Annu Rev Phytopathol. 2002;40:45-74.
737 27. Smith ML, Lindbo JA, Dillard-Telm S, Brosio PM, Lasnik AB, McCormick AA, et
738 al. Modified tobacco mosaic virus particles as scaffolds for display of protein antigens for
739 vaccine applications. Virology. 2006;348(2):475-88.
740 28. Hassani-Mehraban A, Creutzburg S, van Heereveld L, Kormelink R. Feasibility of
741 Cowpea chlorotic mottle virus-like particles as scaffold for epitope presentations. Bmc
742 Biotechnol. 2015;15.
743 29. Speir JA, Munshi S, Wang G, Baker TS, Johnson JE. Structures of the native and
744 swollen forms of cowpea chlorotic mottle virus determined by X-ray crystallography and
745 cryo-electron microscopy. Structure1995. p. 63-78.
746 30. Adolph KW, Butler PJ. Studies on the assembly of a spherical plant virus. I. States of
747 aggregation of the isolated protein. Journal of molecular biology. 1974;88(2):327-41.
748 31. Zeltins A, West J, Zabel F, El Turabi A, Balke I, Haas S, et al. Incorporation of
749 tetanus-epitope into virus-like particles achieves vaccine responses even in older recipients in
750 models of psoriasis, Alzheimer's and cat allergy. NPJ Vaccines. 2017;2:30.
751 32. Fox JM, Zhao X, Speir JA, Young MJ. Analysis of a salt stable mutant of cowpea
752 chlorotic mottle virus. Virology: Academic Press Inc.; 1996. p. 115-22.
753 33. Jennings GT, Bachmann MF. The coming of age of virus-like particle vaccines. Biol
754 Chem. 2008;389(5):521-36.
755 34. A CG, Roesti ES, El-Turabi A, Bachmann MF. Type of RNA Packed in VLPs
756 Impacts IgG Class Switching-Implications for an Influenza Vaccine Design. Vaccines
757 (Basel). 2019;7(2).
758 35. Bessa J, Bachmann MF. T cell-dependent and -independent IgA responses: role of
759 TLR signalling. Immunol Invest. 2010;39(4-5):407-28.
760 36. Jegerlehner A, Maurer P, Bessa J, Hinton HJ, Kopf M, Bachmann MF. TLR9
761 signaling in B cells determines class switch recombination to IgG2a. J Immunol.
762 2007;178(4):2415-20.
763 37. Bessa J, Jegerlehner A, Hinton HJ, Pumpens P, Saudan P, Schneider P, et al. Alveolar
764 macrophages and lung dendritic cells sense RNA and drive mucosal IgA responses. J
765 Immunol. 2009;183(6):3788-99.
766 38. Bachmann MF, Jennings GT. Vaccine delivery: a matter of size, geometry, kinetics
767 and molecular patterns. Nat Rev Immunol. 2010;10(11):787-96.
768 39. Carrasco YR, Batista FD. B cells acquire particulate antigen in a macrophage-rich
769 area at the boundary between the follicle and the subcapsular sinus of the lymph node.
770 Immunity. 2007;27(1):160-71.
771 40. Reddy ST, van der Vlies AJ, Simeoni E, Angeli V, Randolph GJ, O'Neil CP, et al.
772 Exploiting lymphatic transport and complement activation in nanoparticle vaccines. Nat
773 Biotechnol. 2007;25(10):1159-64.

41. Berk DA, Swartz MA, Leu AJ, Jain RK. Transport in lymphatic capillaries. II. Microscopic velocity measurement with fluorescence photobleaching. Am J Physiol. 1996;270(1 Pt 2):H330-7.
42. Manolova V, Flace A, Bauer M, Schwarz K, Saudan P, Bachmann MF. Nanoparticles target distinct dendritic cell populations according to their size. Eur J Immunol. 2008;38(5):1404-13.
43. Manolova V, Flace A, Bauer M, Schwarz K, Saudan P, Bachmann MF. Nanoparticles target distinct dendritic cell populations according to their size. European Journal of Immunology. 2008;38(5):1404-13.
44. Keller SA, Bauer M, Manolova V, Muntwiler S, Saudan P, Bachmann MF. Cutting edge: limited specialization of dendritic cell subsets for MHC class II-associated presentation of viral particles. J Immunol. 2010;184(1):26-9.
45. Louie DAP, Liao S. Lymph Node Subcapsular Sinus Macrophages as the Frontline of Lymphatic Immune Defense. Frontiers in Immunology. 2019;10.
46. Mohsen MO, Speiser DE, Knuth A, Bachmann MF. Virus-like particles for vaccination against cancer. Wiley Interdiscip Rev Nanomed Nanobiotechnol. 2020;12(1):e1579.
47. Jegerlehner A, Storni T, Lipowsky G, Schmid M, Pumpens P, Bachmann MF. Regulation of IgG antibody responses by epitope density and CD21-mediated costimulation. Eur J Immunol. 2002;32(11):3305-14.
48. Eckl-Dorna J, Batista FD. BCR-mediated uptake of antigen linked to TLR9 ligand stimulates B-cell proliferation and antigen-specific plasma cell formation. Blood. 2009;113(17):3969-77.
49. Hou B, Saudan P, Ott G, Wheeler ML, Ji M, Kuzmich L, et al. Selective utilization of toll-like receptor and Myd88 signaling in B cells for enhancement of the antiviral germinal center response. Immunity: NIH Public Access; 2011. p. 375-84.
50. Gomes AC, Roesti ES, El-Turabi A, Bachmann MF. Type of RNA packed in VLPs impacts IgG class switching—implications for an influenza vaccine design. Vaccines: MDPI AG; 2019.
51. Willard-Mack CL, Elmore SA, Hall WC, Harleman J, Kuper CF, Losco P, et al. Nonproliferative and Proliferative Lesions of the Rat and Mouse Hematolymphoid System. Toxicologic Pathology. 2019;47(6):665-783.
52. Elmore SA. Histopathology of the Lymph Nodes. Toxicologic Pathology. 2006;34(5):425-54.
53. Lok LSC, Dennison TW, Mahbubani KM, Saeb-Parsy K, Chilvers ER, Clatworthy MR. Phenotypically distinct neutrophils patrol uninfected human and mouse lymph nodes. Proc Natl Acad Sci U S A. 2019;116(38):19083-9.